

Short communication

Catalytic oxidation of trichloroethylene over TiO₂ supported ruthenium catalysts



Jian Wang^{a,b}, Xiaolong Liu^{a,*}, Junlin Zeng^{a,c}, Tingyu Zhu^{a,*}

^a Beijing Research Centre of Process Pollution Control, National Engineering Laboratory for Hydrometallurgical Cleaner Production Technology, Institute of Process Engineering, Chinese Academy of Sciences, Beijing 100190, China

^b University of Chinese Academy of Sciences, Beijing 100049, China

^c School of Chemistry and Chemical Engineering, Guizhou University, Guiyang, Guizhou 550025, China

ARTICLE INFO

Article history:

Received 23 September 2015

Received in revised form 8 December 2015

Accepted 15 December 2015

Available online 17 December 2015

Keywords:

Ruthenium

Ru/TiO₂

Catalytic oxidation

Trichloroethylene

Support effect

ABSTRACT

Different types of TiO₂ (anatase, P25 and rutile) supported ruthenium catalysts were synthesized by wet impregnation and directly reduced in H₂. The distribution characteristics of ruthenium species were thoroughly studied before and after trichloroethylene oxidation. The results show that ruthenium oxide species are very unstable in the anatase phase, but quite stable in the rutile phase of TiO₂. This phenomenon results in different catalytic behaviors for the Ru/TiO₂ catalysts. The Ru/TiO₂ (P25) catalyst has the best catalytic performance among these catalysts. The complete conversion temperature of trichloroethylene is in the temperature range of 260–270 °C.

© 2015 Elsevier B.V. All rights reserved.

1. Introduction

Volatile organic compounds (VOCs) are toxic and may cause a series of environmental problems [1]. Catalytic oxidation is preferred for the abatement of VOCs, because it does not implement the transfer of pollutants but complete decomposition [2]. In the past decade, efforts have been made to investigate the prospect of ruthenium-based catalysts for the catalytic oxidation of VOCs, due to the low price and fascinating properties of ruthenium [3–6]. Although the ruthenium-based catalysts show high activities, catalyst deactivation is also widely reported [4,6].

However, the knowledge about active state of ruthenium for oxidation reactions is mostly obtained through CO oxidation over ideal single crystal surfaces because of the simplicity [7–14]. The main viewpoints can be summarized as follows:

- (i) Peden and Goodman [7] suggested that the Ru(0001)-(1 × 1) oxygen surface is active for CO oxidation, and the formation of RuO₂ causes deactivation.
- (ii) Böttcher et al. [8,9] proposed that a so called transient surface oxide (TSO) is active, which can be described as oxygen after completion of the Ru(0001)-(1 × 1) oxygen structure but before the formation of ordered RuO₂.

- (iii) Over et al. [10–14] provided ample evidences that CO can be strongly adsorbed on the coordinatively unsaturated Ru sites (Ru_{cus}) of RuO₂(110) and RuO₂(100)-c(1 × 1) surface, and oxygen atom on the bridge site (O_{br}) or on-top site (O_{ot}) will react with adsorbed CO. The activity loss is caused by phase transformation of the active RuO₂ to an inert RuO₂(100)-c(2 × 2) structure (without Ru_{cus} sites). And the RuO₂(100)-c(2 × 2) is formed by surface reconstruction of RuO₂(100)-c(1 × 1).

Obviously, these conclusions are not fully consistent. Therefore, there are heavy debates on the understanding regarding the activation and the deactivation mechanism regarding actual ruthenium-based catalysts [15–21]. The results of Rosenthal et al. [22] indicate that the behavior of polycrystalline Ru/RuO₂ is very complicated, and the above mechanism may coexist. Although the initial activities of ruthenium may decrease, it has been reported that stable states can be eventually achieved for ruthenium-based materials under relatively low temperature (e.g., <400 °C) in total oxidation reactions [3–5]. Thus, ruthenium-based catalysts are promising candidates for the catalytic oxidation of VOCs.

Debecker et al. [6] reported a nano-RuO₂/TiO₂ catalyst for propane oxidation. They found that the homogeneously distributed RuO₂ particles migrate from anatase to rutile phase of TiO₂ at over 150 °C. Because most of the applied noble metal catalysts are supported to increase the exposure of active components, and also because TiO₂ is an important

* Corresponding authors.

E-mail addresses: liuxl@ipe.ac.cn (X. Liu), tyzhu@ipe.ac.cn (T. Zhu).

commercial catalyst support, a clear understanding of the support effect in TiO₂ is important. The migration of ruthenium oxide species may have a great influence on the catalytic performance because ruthenium is easy to be oxidized. And to the best of our knowledge, no studies concerning the support effect in different types of TiO₂ supported ruthenium catalysts for VOC oxidation have been reported.

In this article, Ru/TiO₂ catalysts using different types of TiO₂ (anatase, P25 and rutile) as the supports were synthesized. Activity evaluations and long-term stability tests were conducted for trichloroethylene oxidation. The results suggest that the catalytic performance is greatly influenced by the supports, which is due to the migration of ruthenium oxide species.

2. Experimental

2.1. Catalyst preparation and characterization

Three types of TiO₂ were calcined at 500 °C for 2 h. The resultant materials, referred to as Anatase (Aladdin, >99.5%; average particle size, 21 nm; specific surface area, 62.4 m²/g; anatase), P25 (Degussa, >99.5%; average particle size, 24 nm; specific surface area, 51.3 m²/g; anatase/rutile ≈ 84/16) and Rutile (Aladdin, >99.8%; average particle size, 40 nm; specific surface area, 31.8 m²/g; rutile) were used as the supports, and Ru(NO)(NO₃)₃ (1.5 mg/mL, Alfa-Aesar) was used as the ruthenium precursor. Briefly, the respective TiO₂ particles were stirred with Ru(NO)(NO₃)₃ in solution at room temperature. After impregnation, the samples were dried and reduced in a 5 vol.% H₂/Ar stream at 450 °C for 6 h, affording TiO₂ supported ruthenium catalysts denoted as Ru_x(WI_{R-450})/Support, where *x* is the weight percentages of Ru (calculated), and Support is the type of TiO₂ used.

The ruthenium content was verified by an inductively coupled plasma-optical emission spectrometer (ICP-OES, Optima 5300DV, Perkin Elmer). The porous texture was characterized by N₂ adsorption at 77 K in an automatic surface area and porosity analyzer (Autosorb iQ, Quantachrome). The X-ray diffraction (XRD) patterns were recorded on a powder diffractometer (Rigaku D/Max-RA) using Cu Kα radiation (40 kV and 120 mA). Transmission electron microscope (TEM), high-resolution TEM (HR-TEM) were used with a FEI Tecnai G2 F20 field emission electron microscope operating at 200 kV, and X-ray photoelectron spectroscopy (XPS) measurements were made on a photoelectron spectrometer (ESCALAB 250, Thermo Scientific) by using AlKα (1486.8 eV) radiation as the excitation source (powered at 10 mA and 15 kV).

2.2. Catalytic oxidation of trichloroethylene

Catalytic reactions were carried out in a quartz tube, single-pass fixed-bed micro reactor (4 mm i.d.) with a sieve plate in the middle. The catalyst mixed with quartz sands was placed on the sieve plate. The reactor was heated by an electric furnace, and the temperature was monitored through a K-type thermocouple next to the catalyst bed. Trichloroethylene/Ar was introduced from a gas cylinder, while water vapor was introduced by passage of Ar through a heated saturator. The reactant and products (CO₂, CO and organic by-products) were on-line analyzed with a gas chromatograph (GC 2010, Shimadzu) equipped with a methanizer (MTN, Shimadzu) and two flame ionization detectors, and off-line with a gas chromatograph–mass spectrometer (GCMS-QP2010 Plus, Shimadzu). The inlet concentration of trichloroethylene was calibrated at 500 ± 5 ppm through a by-pass.

The conversion of trichloroethylene was calculated using Eq. (1) and CO₂ as well as CO yield was defined by Eq. (2), respectively.

$$X = \frac{C(\text{in}) - C(\text{out})}{C(\text{in})} \times 100\% \quad (1)$$

$$\text{CO}_x \text{ yields} = \frac{C(\text{CO}_x)}{2 \times C(\text{in})} \times 100\% (x = 1, 2) \quad (2)$$

where *X* is the conversion, *C*(in) and *C*(out) are the inlet and outlet concentration of the gaseous reactant and *C*(CO_{*x*}) (*x* = 1, 2) is the outlet concentration of CO₂ or CO (when mentioned as CO_{*x*} it is the summation of these products).

The concentrations of HCl were on-line measured with a Fourier transform infrared spectrometer (Nicolet 6700, Thermo Scientific) equipped with a 2 m optical path gas cell. And the concentrations of Cl₂ were calculated by the effluent stream bubbling through a 0.0125 M NaOH solution followed by titration with ferrous ammonium sulfate (FAS) using N,N-diethyl-*p*-phenylenedi-amine (DPD) as indicator [23].

3. Results and discussion

Table 1 shows the characterization data for various samples. The *S*_{BET} of the fresh catalysts decrease slightly compared with the supports. And it was found that the actual ruthenium contents of the catalysts are similar to the calculated values (within the error range). The XRD patterns of the Ru/TiO₂ catalysts (Fig. S1) reveal pure anatase phase and rutile phase for the Ru₁(WI_{R-450})/Anatase and Ru₁(WI_{R-450})/Rutile catalysts, respectively. And the data of the Ru₁(WI_{R-450})/P25 catalyst shows typical binary phases. No diffraction peaks assignable to ruthenium species can be found among these catalysts. TEM characterization for the Ru/TiO₂ catalysts was obtained. As shown in Fig. 1, ruthenium particles are homogeneously distributed, but the average particle size of metallic ruthenium for each catalyst is not the same, which is between 1 and 2 nm (Table 1). Generally, the ruthenium particles on the support with larger *S*_{BET} are smaller compared with those on the support with smaller *S*_{BET}.

The results of these catalysts for trichloroethylene oxidation are shown in Fig. 2. The activity evaluation was carried out by heating at 1 °C/min and repeated for several cycles. The carbon balance (± 1%) could be fulfilled when the temperature was above 150 °C. Fig. 2a shows that the activity of the Ru₁(WI_{R-450})/Anatase catalyst decreases in each run. And the CO_{*x*} yields are not equal to trichloroethylene conversions, indicating the formation of organic by-products with a maximum amount of about 20%. Fig. 2b shows that the Ru₁(WI_{R-450})/P25 catalyst can finally achieve stable-states as indicated by the catalytic performance of the third and fourth runs. Again, the CO_{*x*} yields of this catalyst are also much lower than the trichloroethylene conversions in the temperature range of 210–260 °C. As for the Ru₁(WI_{R-450})/Rutile catalyst (Fig. 2c), the activity decreases continuously after each run. But the extent of the decline is quite small after the first run. And it is interesting that the formation of the organic by-products is obviously decreased.

Long-term stability tests for these catalysts after activity evaluations were performed. As shown in Fig. 3, the conversion of trichloroethylene over the Ru₁(WI_{R-450})/Anatase catalyst decreases substantially with

Table 1
Characterization data for various samples.

Catalyst	Ruthenium content (wt.%) ^a	<i>S</i> _{BET} (m ² /g) ^b	Pore volume (cm ³ /g) ^c	<i>d</i> _{Ru} (nm) ^d
Ru ₁ (WI _{R-450})/Anatase	1.0 (0.98)	60.2	0.41	1.1
Ru ₁ (WI _{R-450})/P25	1.0 (1.02)	49.7	0.51	1.4
Ru ₁ (WI _{R-450})/Rutile	1.0 (1.05)	29.6	0.18	2.0
Ru ₁ (WI _{R-450})/Anatase (used)	1.0 (1.03)	61.2	0.39	1–20
Ru ₁ (WI _{R-450})/P25 (used)	1.0 (1.05)	49.1	0.52	2–7
Ru ₁ (WI _{R-450})/Rutile (used)	1.0 (1.01)	30.1	0.18	2–3

^a The data in the parentheses show the accurate values.

^b The specific surface area (*S*_{BET}) was calculated from the N₂ adsorption isotherm using the Brunauer-Emmett-Teller (BET) equation.

^c The pore volume was determined from the N₂ desorption isotherm using the Barrett-Joyner-Halenda (BJH) method.

^d The average particle size of ruthenium (*d*_{Ru}) was determined after the used catalysts being reduced in H₂.

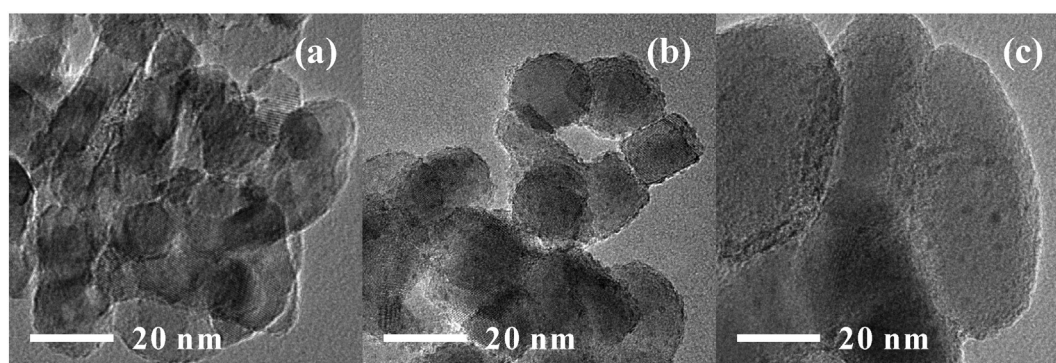


Fig. 1. TEM micrographs of the Ru/TiO₂ catalysts. (a) Ru₁(WI_{R-450})/Anatase. (b) Ru₁(WI_{R-450})/P25. (c) Ru₁(WI_{R-450})/Rutile.

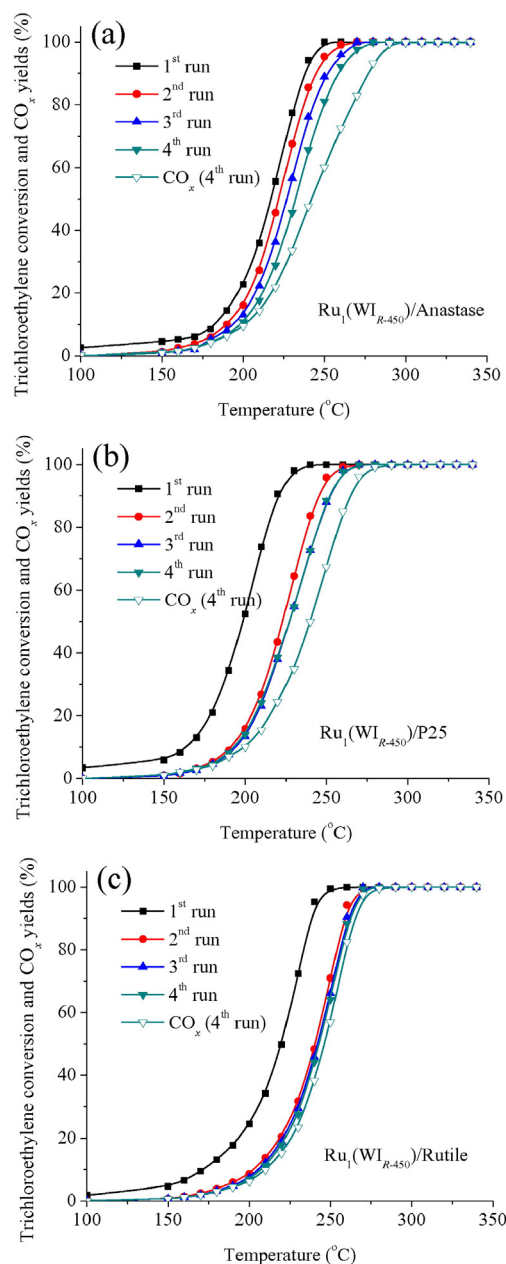


Fig. 2. Trichloroethylene conversion as a function of temperature for the Ru/TiO₂ catalysts (500 ppm trichloroethylene, 20 vol.% O₂, balance Ar; 100 mg catalyst; WHSV 60,000 mL g⁻¹ h⁻¹, 1 °C/min).

time. In contrast, the activity of the Ru₁(WI_{R-450})/P25 catalyst is stable. These observations are consistent with the above temperature cycle results. However, the activity of the Ru₁(WI_{R-450})/Rutile catalyst decreases at first, but then increases slightly. Nevertheless, no obvious changes can be observed in ruthenium content, S_{BET} and pore volume of the used catalysts compared with the fresh ones (Table 1). Therefore, the used catalysts were characterized by TEM (Fig. S2), but ruthenium species cannot be found. And it is because of that, the metallic ruthenium is oxidized into ruthenium oxide species (see the XPS results in Fig. S3), which often have a low contrast.

Hence, the used catalysts were reduced in a 5 vol.% H₂/Ar flow at 300 °C, and then characterized by TEM and HR-TEM as shown in Fig. 4. In Fig. 4a, the used Ru₁(WI_{R-450})/anatase catalyst shows significant sintering (some small ruthenium particles still exist). It should be pointed out that the ruthenium species of the used catalysts are oxidized, and the severely sintered Ru₁(WI_{R-450})/anatase catalyst shows the diffraction peaks of RuO₂ (Fig. S1). In Fig. 4c, it is also found that aggregation of ruthenium species occurs for the used Ru₁(WI_{R-450})/P25 catalyst, but this system can be described as moderate sintering. Fig. 4d shows clear lattice fringes of the TiO₂ particles and metallic ruthenium (corresponding to the yellow dotted line area in Fig. 4c). The lattice spacing of the sample with ruthenium is 0.21 nm, and the lattice spacing of the sample containing a few ruthenium species is 0.35 nm, which is consistent with that of the rutile (210) and anatase (101) crystal planes of TiO₂, respectively. Therefore, the ruthenium species are mostly distributed in the rutile phase of P25, and the ruthenium oxide species can be described as being captured by the rutile phase of P25 (about 20% of the P25-TiO₂ is the rutile phase). In Fig. 4e, there is only a small degree of sintering for the Ru₁(WI_{R-450})/Rutile catalyst. These results indicate that the rutile phase of TiO₂ can better maintain the original morphology of ruthenium oxide species.

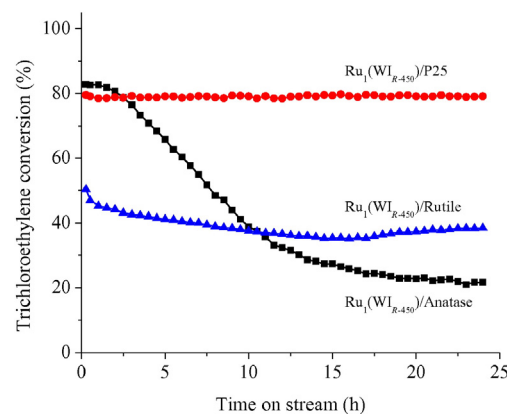


Fig. 3. Long-term stability tests for the Ru/TiO₂ catalysts at 240 °C (500 ppm trichloroethylene, 20 vol.% O₂, balance Ar; 100 mg catalyst; WHSV 60,000 mL g⁻¹ h⁻¹).

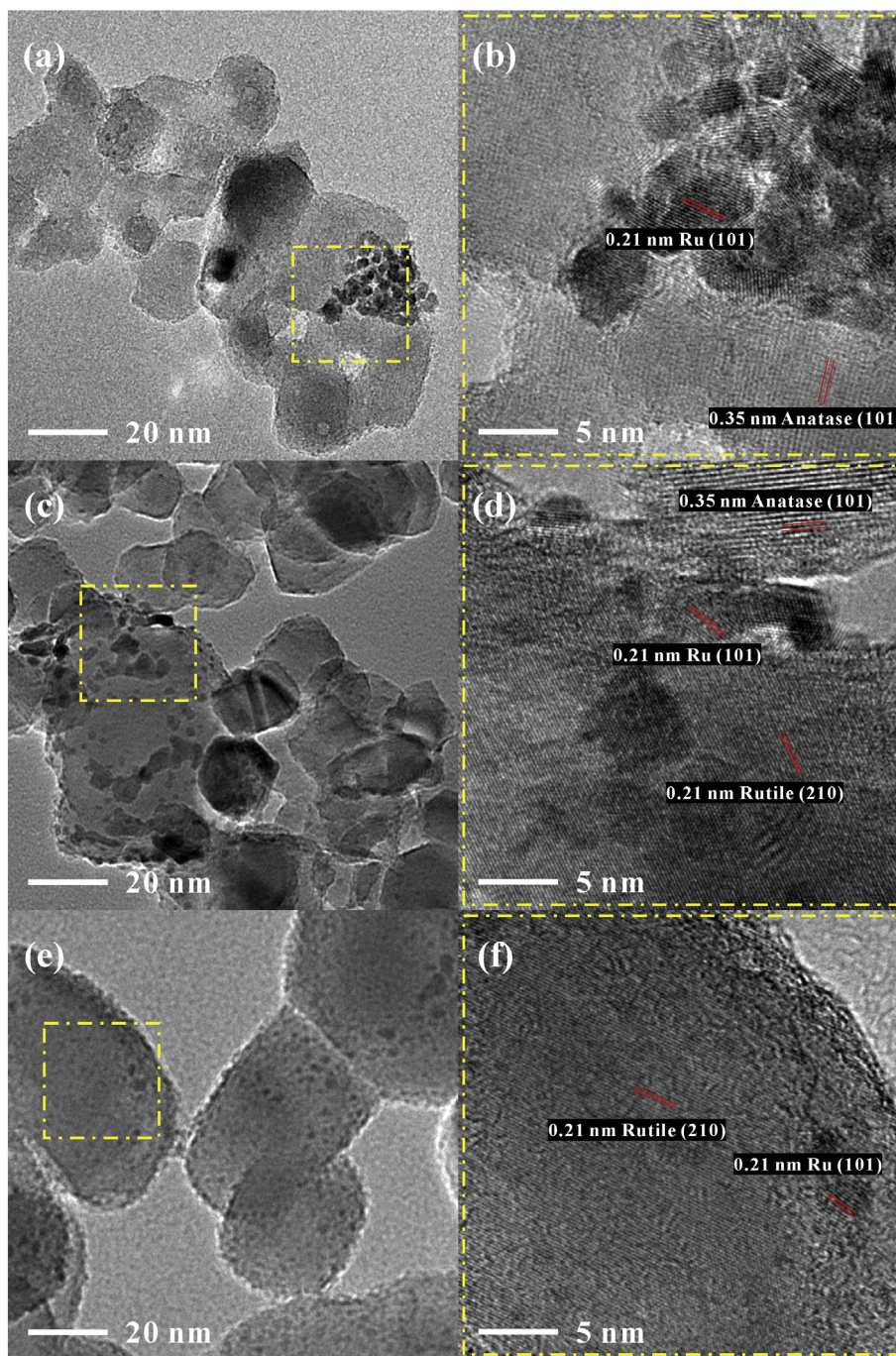


Fig. 4. TEM and HR-TEM micrographs of the used Ru/TiO₂ catalysts after reduction. (a–b) Ru₁(WI_{R-450})/Anatase. (c–d) Ru₁(WI_{R-450})/P25. (e–f) Ru₁(WI_{R-450})/Rutile.

As suggested by Over et al. [16], the deactivation of ruthenium species can be attributed to the formation of the inert RuO₂(100)-c(2 × 2) structure. So the initial activity losses for the Ru/TiO₂ catalysts could have resulted from the oxidation in the activity evaluations, and chlorination of the catalysts may also play an important role. But the Ru₁(WI_{R-450})/P25 catalyst can eventually achieve stable states. Hence, this indicates that the activity changes for the other two catalysts are caused by the migration of ruthenium oxide species. The ruthenium oxide species are quite unstable in the anatase phase of TiO₂, but quite stable in the rutile phase. A reasonable explanation is that, the rutile phase of TiO₂ has plenty of lattice defects on the surface and shares similar crystal cell parameters with RuO₂, thus the interaction between them is extremely strong [24]. Therefore, the stability of Ru₁(WI_{R-450})/Anatase catalyst is poor compared with that of the Ru₁(WI_{R-450})/P25 and

Ru₁(WI_{R-450})/Rutile catalysts because of being severely sintered. However, the ruthenium oxide species of the Ru₁(WI_{R-450})/Rutile catalyst seem to undergo slow sintering even at the end of the stability test, because the particle sizes of the ruthenium oxide species of this catalyst are very small. The migration of ruthenium oxide species in the rutile phase of TiO₂ does not occur when the particle size of ruthenium oxide species is above 2–3 nm. So the Ru₁(WI_{R-450})/P25 catalyst exhibits the highest stability.

Another interesting phenomenon is that, the activity of the Ru₁(WI_{R-450})/Rutile catalyst which has the best ruthenium dispersion is lower than that of the Ru₁(WI_{R-450})/P25 catalyst. This phenomenon can be explained through particle size effect which may exist in ruthenium oxide species. For instance, Pt⁰ atoms exposed to the outmost layer of large Pt⁰ particles are far more active than the ones in the

same position of small Pt⁰ particles [25] because the abilities to activate the reactants are stronger. Thus, it is possible that the catalyst with large metal or metal oxide particles is more active than that with small ones, even though the latter exposes more active sites. Sintering will reduce the number of the active sites on the one hand and change (speculatively increase) the activities of the ruthenium oxide species exposed on the outmost layer on the other hand. Hence, the combined effects lead to the change of the activities for the Ru/TiO₂ catalysts. Therefore, the activity of the Ru₁(W_{R-450})/Anatase catalyst is the lowest due to lack of active sites, and the Ru₁(W_{R-450})/P25 catalyst is more active than the Ru₁(W_{R-450})/Rutile catalyst because of the moderate sintering. It can also be noticed that the Ru₁(W_{R-450})/Anatase and Ru₁(W_{R-450})/P25 catalysts produce more by-products than the Ru₁(W_{R-450})/Rutile catalyst (Fig. 2), indicating that the large ruthenium oxide particles may act as “moderate” adsorption sites. These results suggest that particle size effect exists for ruthenium oxide species. And it also indicates that the activity of a rutile-TiO₂ supported ruthenium catalyst can be promoted by altering the particle size of ruthenium species.

Generally, water vapor exists in the inlet feed of VOCs when a catalyst is actually applied, which may have great effects [26]. Therefore, we studied the effects of water vapor on trichloroethylene oxidation over the Ru₁(W_{R-450})/P25 catalyst as shown in Fig. 5. The selectivity to chlorinated by-products can be deduced from the differences between the trichloroethylene conversions and CO_x yields at various temperatures. In the absence of additional water vapor (Fig. 5a), CO₂ holds an absolutely majority in the CO_x yields, but tens of ppm of CO can also be detected, and approximately 25% of the trichloroethylene is converted to organic by-products in the outlet stream at 230 °C. With the increase of temperature, the ratio of HCl in inorganic chlorine decreases to about 10%, and the organic by-products mainly consist of

tetrachloroethylene and a small amount of pentachloroethane (Fig. 5b). In the presence of additional water vapor (Fig. 5c), it can be observed that the activity of the catalyst is suppressed, and a reasonable explanation is that the additional water vapor can compete with the reactants (trichloroethylene and O₂) for the active sites. However, the CO_x yields are almost equal to the trichloroethylene conversions in the whole studied temperature, and there is hardly any CO that can be detected. Meanwhile, the ratio of HCl in inorganic chlorine increases compared with that in the absence of additional water vapor (Fig. 5d), but the overall trend is not changed. Besides, the formation of the organic by-products (especially tetrachloroethylene) is greatly reduced. Compared with the one used in the absence of additional water vapor, no obvious changes in ruthenium oxide species can be found, but the organic and inorganic chlorine species are reduced (Fig. S3 and Table S1). These results indicate that the chlorine species on the catalyst surface can be removed by water vapor. Thus, it will inhibit the formation of the organic by-products. The formation of pentachloroethane may be due to the tetrachloroethylene and HCl addition or trichloroethylene and Cl₂ addition, so the introduction of additional water vapor will change the relative ratios of the by-products. Based on the above results, the major effects of water vapor on the reaction can be summarized as follows: (i) compete with the reactants for the active sites; (ii) improve the selectivities to CO_x and HCl; and (iii) change the relative ratios of the organic by-products.

As shown in Table 2, the 90% conversion temperature (*T*₉₀) of trichloroethylene over the Ru₁(W_{R-450})/P25 catalysts is much lower than that of the previously reported catalysts even in the case of the highest space velocity. Co is easy to combine with chlorine, resulting in the activity losses. The advantage of V₂O₅/TiO₂ catalysts in the catalytic oxidation of Cl-VOCs is that VO_x species have a strong ability to resist

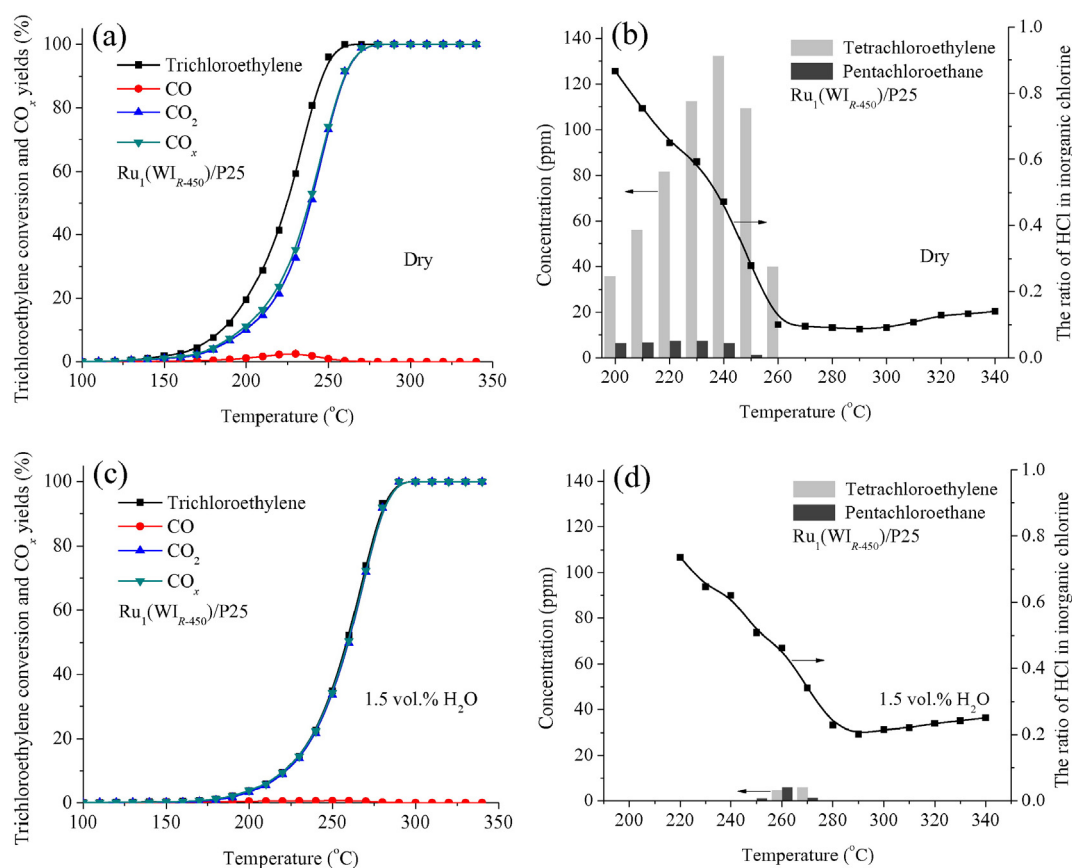


Fig. 5. Trichloroethylene conversion, CO_x yields, distribution of the organic by-products and ratio of HCl in inorganic chlorine as a function of temperature over the Ru₁(W_{R-450})/P25 catalyst in the (a–b) absence and (c–d) presence of additional water vapor (1.5 vol.%). (500 ppm trichloroethylene, 20 vol.% O₂, balance Ar; 100 mg catalyst; WHSV 60,000 mL g⁻¹ h⁻¹, steady-states).

Table 2
Data of research articles on trichloroethylene oxidation.

Catalyst	Concentration (ppm)	WHSV (mL g ⁻¹ h ⁻¹)	T ₉₀ (°C)	Ref. no.
Co ₂ AlO _x	1000	35,300	340	[32]
3.5 wt.% V ₂ O ₅ /TiO ₂	1000	30,000	372	[33]
0.5 wt.% Pt/γ-Al ₂ O ₃	1091	46,800	495	[34]
0.5 wt.% Ru/γ-Al ₂ O ₃	1091	46,800	375	[35]
1 wt.% Ru/TiO ₂ (P25)	500	60,000	249	This work

chlorine poisoning. But the catalytic activities of these catalysts are relatively low, giving a large amount of CO as one of the oxidation products [27,28]. Pt-based materials exhibit high activities in the catalytic oxidation of non-chlorinated VOCs, but the activities of these catalysts are also strongly inhibited by chlorine. For example, the total conversion temperature (T₁₀₀) of toluene over a Pt/γ-Al₂O₃ catalyst can be lower than 230 °C [29], but the T₁₀₀ of chlorobenzene is above 375 °C [27]. According to the previous report [3], the Ru/γ-Al₂O₃ catalyst will show severe sintering during the calcination or oxidation process, which is very similar with the Ru₁(W_{R-450})/Anatase catalyst, thus γ-Al₂O₃ is not a good catalyst support for ruthenium species in oxidation reactions at high temperature. Therefore, the Ru₁(W_{R-450})/P25 catalyst reported in this paper can retain a relatively good dispersion of ruthenium oxide species, and also because ruthenium oxide species can effectively remove chlorine from the active sites (industrially applied as active species for the Deacon process, 2 HCl + 1/2 O₂ = Cl₂ + H₂O [24]), thus having good performance in the catalytic oxidation of trichloroethylene. In this work, the fresh catalysts with relatively small particles of metallic ruthenium were fully oxidized (Fig. S3). With Cl-VOCs as reactants, the ruthenium oxide species are chlorinated, so the active species can be described as chlorinated ruthenium oxide species. Over et al. [30] reported RuO₂ as active species for the Deacon process and suggested that O_{br} of RuO₂ can be replaced by Cl. Meanwhile, the adsorbed HCl and O₂ (dissociated into O atoms) on Ru_{cus} sites can react with each other through the Langmuir–Hinshelwood mechanism [31]. We believe that the Deacon process and the reaction proposed in this article may possess a similar pathway. The verification test is currently being performed in our laboratory.

4. Conclusions

Different types of TiO₂ (anatase, P25 and rutile) supported ruthenium catalysts with homogeneously distributed ruthenium particles were synthesized. These catalysts are very active for trichloroethylene oxidation, but it was found that ruthenium oxide species formed during the reaction are very unstable in the anatase phase of TiO₂. The rutile phase of TiO₂ has a similar structure with RuO₂, thus better maintaining the morphology of ruthenium oxide species. And particle size effect exists for ruthenium-based materials. Besides, the existence of additional water vapor will increase the formation of HCl and greatly reduce the amount of tetrachloroethylene and pentachloroethane as the organic by-products, but also suppress the catalytic activity.

Acknowledgments

This work was supported by the Strategic Priority Research Program of the Chinese Academy of Sciences (No. XDB05050100) and the National Natural Science Foundation of China (No. 21207132).

Appendix A. Supplementary data

Supplementary data to this article can be found online at <http://dx.doi.org/10.1016/j.catcom.2015.12.015>.

References

- R. Seco, J. Penuelas, I. Filella, *Atmos. Environ.* 41 (2007) 2477–2499.
- F. Bertinchamps, C. Gregoire, E.M. Gaigneaux, *Appl. Catal. B Environ.* 66 (2006) 10–22.
- T. Mitsui, K. Tsutsui, T. Matsui, R. Kikuchi, K. Eguchi, *Appl. Catal. B Environ.* 81 (2008) 56–63.
- J. Okal, M. Zawadzki, *Appl. Catal. B Environ.* 89 (2009) 22–32.
- Q. Dai, S. Bai, Z. Wang, X. Wang, G. Lu, *Appl. Catal. B Environ.* 126 (2012) 64–75.
- D.P. Debecker, B. Farin, E.M. Gaigneaux, C. Sanchez, C. Sasso, *Appl. Catal. A Gen.* 481 (2014) 11–18.
- C.H.F. Peden, D.W. Goodman, *J. Phys. Chem.* 90 (1986) 1360–1365.
- A. Bottcher, H. Niehus, S. Schwegmann, H. Over, G. Ertl, *J. Phys. Chem. B* 101 (1997) 11185–11191.
- A. Bottcher, M. Rogozia, H. Niehus, H. Over, G. Ertl, *J. Phys. Chem. B* 103 (1999) 6267–6271.
- H. Over, Y.D. Kim, A.P. Seitsonen, S. Wendt, E. Lundgren, M. Schmid, P. Varga, A. Morgante, G. Ertl, *Science* 287 (2000) 1474–1476.
- Y.D. Kim, S. Schwegmann, A.P. Seitsonen, H. Over, *J. Phys. Chem. B* 105 (2001) 2205–2211.
- Y.D. Kim, A.P. Seitsonen, S. Wendt, J. Wang, C. Fan, K. Jacobi, H. Over, G. Ertl, *J. Phys. Chem. B* 105 (2001) 3752–3758.
- M. Knapp, A.P. Seitsonen, Y.D. Kim, H. Over, *J. Phys. Chem. B* 108 (2004) 14392–14397.
- Y.B. He, M. Knapp, E. Lundgren, H. Over, *J. Phys. Chem. B* 109 (2005) 21825–21830.
- H. Over, M. Muhler, *Prog. Surf. Sci.* 72 (2003) 3–17.
- J. Assmann, D. Crihan, M. Knapp, E. Lundgren, E. Loffler, M. Muhler, V. Narkhede, H. Over, M. Schmid, A.P. Seitsonen, P. Varga, *Angew. Chem. Int. Ed.* 44 (2005) 917–920.
- J. Assmann, V. Narkhede, L. Khodeir, E. Loffler, O. Hinrichsen, A. Birkner, H. Over, M. Muhler, *J. Phys. Chem. B* 108 (2004) 14634–14642.
- J. Assmann, V. Narkhede, N.A. Breuer, M. Muhler, A.P. Seitsonen, M. Knapp, D. Crihan, A. Farkas, G. Mellau, H. Over, *J. Phys. Chem. B* 110 (2006) 11439–11442.
- D.W. Goodman, C.H.F. Peden, M.S. Chen, *Surf. Sci.* 601 (2007) L124–L126.
- D.W. Goodman, C.H.F. Peden, M.S. Chen, *Surf. Sci.* 601 (2007) 5663–5665.
- H. Over, M. Muhler, A.P. Seitsonen, *Surf. Sci.* 601 (2007) 5659–5662.
- D. Rosenthal, F. Girgsdies, O. Timpe, R. Blume, G. Weinberg, D. Teschner, R. Schloegl, *Z. Phys. Chem.* 223 (2009) 183–207.
- J.R. González-Velasco, A. Aranzabal, R. López-Fonseca, R. Ferret, J.A. González-Marcos, *Appl. Catal. B Environ.* 24 (2000) 33–43.
- K. Seki, *Catal. Surv. Jpn.* 14 (2010) 168–175.
- N. Radic, B. Grbic, A. Terlecki-Baricevic, *Appl. Catal. B Environ.* 50 (2004) 153–159.
- C.E. Hetrick, F. Patcas, M.D. Amiridis, *Appl. Catal. B Environ.* 101 (2011) 622–628.
- E. Finocchio, G. Ramis, G. Busca, *Catal. Today* 169 (2011) 3–9.
- J. Wang, X. Wang, X. Liu, J. Zeng, Y. Guo, T. Zhu, *J. Mol. Catal. A Chem.* 402 (2015) 1–9.
- L.F. Liotta, M. Ousmane, G. Di Carlo, G. Pantaleo, G. Deganello, A. Boreave, A. Giroir-Fendler, *Catal. Lett.* 127 (2009) 270–276.
- D. Crihan, M. Knapp, S. Zweidingey, E. Lundgren, C.J. Weststrate, J.N. Andersen, A.P. Seitsonen, H. Over, *Angew. Chem. Int. Ed.* 47 (2008) 2131–2134.
- H. Over, *Chem. Rev.* 112 (2012) 3356–3426.
- N. Blanch-Raga, A. Eduardo Palomares, J. Martinez-Triguero, M. Puche, G. Fetter, P. Bosch, *Appl. Catal. B Environ.* 160 (2014) 129–134.
- M. Wu, K.C. Ung, Q.G. Dai, X.Y. Wang, *Catal. Commun.* 18 (2012) 72–75.
- B. Miranda, E. Diaz, S. Ordonez, A. Vega, F.V. Diez, *Appl. Catal. B Environ.* 64 (2006) 262–271.
- B. Miranda, E. Diaz, S. Ordonez, F.V. Diez, *Catal. Commun.* 7 (2006) 945–949.